2nd International Workshop on Microsystems

Sindos Campus, ATEI Thessaloniki, 20 December 2017

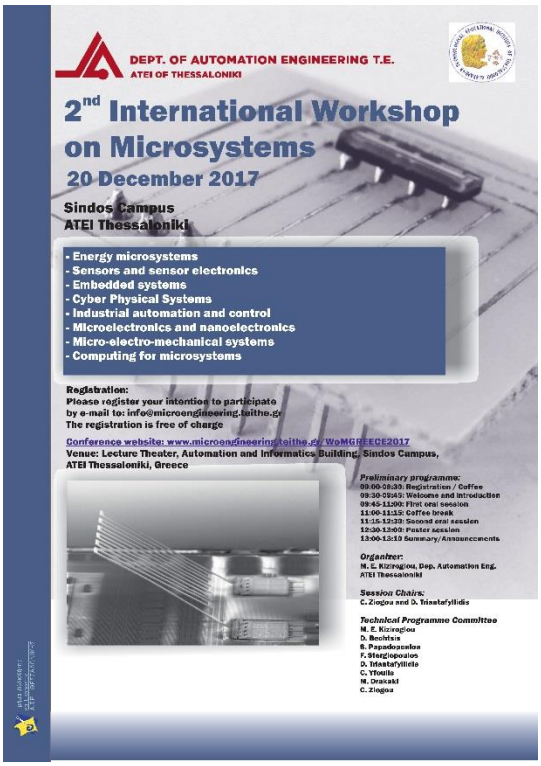

Workshop Proceedings

Introduction

This workshop brings together research and development from a large spectrum of science and engineering fields related to the implementation of microsystems in the new era of distributed information technologies. As cloud computing services and smart portable systems are becoming ubiquitous and more advanced, new possibilities for interdisciplinary research emerge. The microsystems that comprise the so-called internet of things will encompass a wide range of technologies including new energy sources, energy and information electronics, sensor systems, smart and energy efficient control and computing, telecommunications and networking, and also nanotechnology and micro-electro-mechanical systems. Continuing a successful first workshop in 2016, the 2st International Workshop on Microsystems aims at bringing together related research and development advancements from the academic community and the industry. Scientific topics include but are not limited to:

- Energy microsystems
- Sensors and sensor electronics
- Embedded systems
- Cyber Physical Systems
- Industrial automation and control
- Microelectronics and nanoelectronics
- Micro-electro-mechanical systems
- Computing for microsystems

Michail E. Kiziroglou
m.kiziroglou@autom.teithe.gr

Venue

Lecture Theater, Automation and Informatics Building
Sindos Campus, ATEI Thessaloniki, Greece

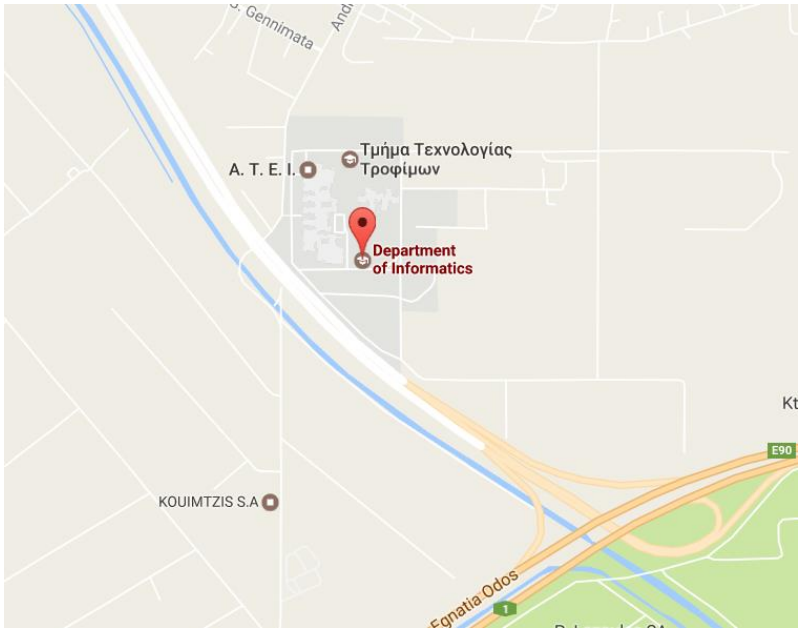

Date

Tuesday, 20th of December, 2017

Organizer

Michail E. Kiziroglou

Session Chairs

Chrisovalantou Ziogou and Dimitris Triantafyllidis

Reviewing Committee

Dimitrios Bechtsis
Maria Drakaki
Chrisovalantou Ziogou
Michail E. Kiziroglou
Simira Papadopoulou
Fotis Stergiopoulos
Dimitris Triantafyllidis
Apostolos Tsagaris
Christos Yfoulis

Organization and Technical Support

Christos Avdimiotis, Maria Pagkrakioti and Kostantinos Pakas

List of Authors

No	Last Name	First Name	Affiliation
1	Bechtsis	Dimitris	ATEI Thessaloniki
2	Hatzikos	Evaggelos V.	ATEI Thessaloniki
3	Kamoutsis	Konstantinos	ATEI Thessaloniki
4	Kiziroglou	Michail E.	ATEI Thessaloniki
5	Papadopoulou	Simira	ATEI Thessaloniki
6	Stergiopoulos	Fotis	ATEI Thessaloniki
7	Triantafyllidis	Dimitris	ATEI Thessaloniki
8	Voutetakis	Spyros	CERTH
9	Yfoulis	Christos	ATEI Thessaloniki
10	Ziogou	Chrysovalantou	CERTH
11	Kolias	Themistoklis	ATEI Thessaloniki
12	Trigkas	Dimitrios	CERTH
13	Kakoulidou	Peristera	ATEI Thessaloniki
14	Eleftheriadou	Kyriaki G.	ATEI Thessaloniki
15	Mpirta	Panagiota A.	ATEI Thessaloniki
16	Papakostas	Dimitrios K.	ATEI Thessaloniki
17	Bazakas	Filippos	AUTH
18	Avdimiotis	Christos	AUTH
19	Mekras	Athanasios	AUTH
20	Papadopoulos	Stylianos-Georgios	AUTH
21	Katselas	Leonidas	AUTH
22	Drakaki	Maria	ATEI Thessaloniki
23	Giannopoulos	Stefanos	ATEI Thessaloniki
24	Vlachogiannis	Georgios	ATEI Thessaloniki
25	Kyriakidis-Tingilidis	Panagiotis	ATEI Thessaloniki
26	Sergentanis	Grigoris	ATEI Thessaloniki
27	Gkagkanis	Efstratios	ATEI Thessaloniki

List of Participating Organizations

Alexander Technological Educational Institute of Thessaloniki, Greece
Aristotle University of Thessaloniki, Greece
Centre for Research and Technology Hellas (CERTH), Greece

Programme

08:45-09:15: Registration

Please check-in or register at the front desk

09:15-09:30: Welcome and introduction

09:30-10:45: First Oral Session (Session Chair: TBS)

09:30: Energy Management and Automation Engineering for Battery Systems, Renewable Hydrogen & Smart Grids. *S. Voutetakis* (Invited, CPERI, CERTH), 17WOM-01

10:00: Energy Management Strategy for Stand-alone Power Production Stations based on RES, Batteries and Hydrogen. *D. Trigkas, C. Ziogou, S. Voutetakis and S. Papadopoulou*, 17WOM-02

10:15: System Identification and Model Order Reduction of a Li-ion Battery and Ultracapacitor Forklift, *P.Kakoulidou, C. Ziogou, C. Yfoulis, S. Voutetakis and S. Papadopoulou*, 17WOM-03

10:30: Smart Home Automation Control and Monitoring System Using Microcontroller and Android Phone, *Th. Kolias, K. Kamoutsis and E. V. Hatzikos*, 17WOM-04

10:45-11:15: Coffee Break and Demo Session

During the coffee break, a demonstrator of paper 17WOM-04 by Kolias et al will be displayed.

11:15-12:45: Second Oral Session (Session Chair: Dimitrios Triantafyllidis)

11:15 Fault Detection Voltage and Current Measurements Comparative Study, *K. G. Eleftheriadou, P. A. Mpirta and D. K. Papakostas*, 17WOM-05

11:30: Embedded infrared building monitoring system, *F. Bazakas, C. Avdimiotis, A. Mekras, S. G Papadopoulos and L. Katselas*, 17WOM-06

11:45: Design and manufacture of voice distortion device in real time, *S. Giannopoulos and M. Drakaki*, 17WOM-07

12:00: An Intelligent Autonomous Vehicle (IAV) prototype for industrial facilities, G. Vlachogiannis, P. Kyriakidis-Tingilidis and D. Bechtsis, 17WOM-08

12:15: DC-Link Capacitor Voltage Balancing in a Three-Phase Neutral Point Clamped Inverter, *G. Sergentanis, F. Stergiopoulos and D. Triantafyllidis*, 17WOM-09

12:30: Driving a Linear Sensor Array of Photodiodes with the use of AM3358 Sitara Processor, *S. Gkagkanis and M. E. Kiziroglou*, 17WOM-10

12:45-13:00: Concluding remarks

WORKSHOP ABSTRACTS

Energy Management and Automation Engineering for Battery Systems, Renewable Hydrogen & Smart Grids

Spyros Voutetakis
Chemical Process and Energy Resources Institute (CPERI), Centre for Research and Technology Hellas (CERTH), Thessaloniki, Greece

The world-wide increasing demand for power, combined with the need for security of energy supply has led to an ongoing effort to shift from the traditional power generation grid to a flexible smart and multi-source power networks that include Renewable Energy Sources (RES) where mainly Photovoltaic panels (PV) or Wind Generators (WG) are the main source of power. As both demand and supply dynamically varies through time, a highly complex environment has emerged. The intermittent nature of RES can be securely managed with the utilization of intermediate storage systems, such as accumulators (battery stacks). Alternatively, hydrogen production, storage and usage through fuel cells can serve the need for continuous availability of power. Overall the operation of such networks and their involved subsystems depends on Energy Management Strategies combined with automation infrastructures for the acquisition of signals from the sensor network and communication protocols for establishing the information exchange between the various heterogeneous subsystems [1].

The main objective is to analyze and suggest an EMS for the management of power and resources of the smart-grid domain and to capitalize on the available technologies and industrial automation protocols (e.g. OPC) [2]. To achieve this goal, the behavior of the involved systems is considered and the requirements for energy management in a dynamic and distributed environment are determined using appropriate automation engineering methods and techniques. The objective of an EMS is to efficiently exchange energy between the involved subsystems, to maximize the use of available stored energy and to exploit the overall power produced by RES. In general the common aspects between the subsystems of different scale, from battery stacks to smart-grid networks, are the online monitoring, the involved industrial-grade automation and the control and optimization methods. Thus, some respective cases will be analysed in this work in order to demonstrate the aforementioned aspects.

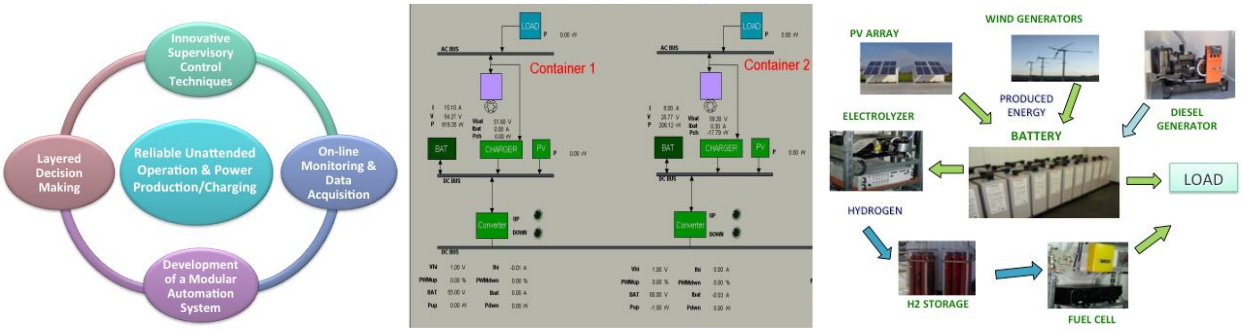

Figure 1. a) conceptual components, b) online monitoring, c) topology of a RES powered station

References

[1] C. Ziogou, D. Ipsakis, C. Elmasides, F. Stergiopoulos, S. Papadopoulou, P. Seferlis, S. Voutetakis, 2011, Automation infrastructure and operation control strategy in a stand-alone power system based on renewable energy sources, Journal of Power Sources, 196 (22), 9488-99

[2] C. Ziogou, S., Voutetakis, S., Papadopoulou, 2016, Design of an energy decision framework for an autonomous RES-enabled smart-grid network, 2016 23rd International Conference on Telecommunications, ICT 2016, art. no. 7500384, 1-5

Energy Management Strategy for Stand-alone Power Production Stations based on RES, Batteries and Hydrogen

D. Trigkas[(1)], C. Ziogou[(1)], S. Voutetakis[(1)], S. Papadopoulou[(1,2)]

[(1)] Chemical Process and Energy Resources Institute (CPERI), Centre for Research and Technology Hellas (CERTH), Thessaloniki, Greece

[(2)] Department of Automation Engineering, Alexander Technological Educational Institute of Thessaloniki, Greece

***Abstract*—The purpose of this work is to study energy management strategies (EMS) for autonomous (Renewable Energy Sources) RES systems. The system into consideration contains a PV array, wind Generators, an electrolyzer, a Proton Exchange Membrane Fuel Cell (PEMFC), Lead Acid batteries, a compressor and hydrogen storage Tanks. Using mathematical models for the components, an EMS is validated for power distribution among the systems fulfilling a load demand for a given time period.**

I. INTRODUCTION

Renewable energy systems are rapidly becoming more efficient and cheaper. Their share in total energy consumption is increasing rapidly. The integration of new methods of energy storage and generation makes it possible to create autonomous grids of power production. Autonomous RES microgrids can be used in electrifying remote areas such as islands, mountainous areas or scientific stations. One of the main concern for the optimal functionality of a RES microgrid in terms of power distribution and maintenance cost is the EMS.

II. SYSTEM TOPOLOGY AND MODELS

The integrated system into consideration consists of two sections. A power generation section that utilizes a photovoltaic array, three wind turbines and a PEM Fuel Cell with subsequent use for alternative power generation. An energy storage section that consists of a lead acid accumulator and a PEM electrolyzer that is used for energy storage in the form of hydrogen. Also power converters are used to connect the sections together utilizing a common DC bus for power distribution and an AC bus for the load and auxiliary devices power demand.

TABLE I
SUBSYSTEMS CHARACTERISTICS OF THE AUTONOMOUS MICROGRID

PV arrays	Wind generators	Lead-Acid accumulator	PEM fuel cell	PEM electrolyzer	Storage tanks
5KWp	3KWp	1000Ah	4KWp	4.2KWp	0.3/0.6m^3

A Proton-Exchange Membrane Fuel Cell (PEMFC) is an electrochemical device that converts chemical energy stored in hydrogen to electrical energy and water. On the other hand a PEM Electrolyzer is an electrochemical device that converts electrical energy to hydrogen and oxygen. The hydrogen that is produced from the electrolyzer is stored and it can be used from the fuel cell.

In order to study the behavior of the autonomous RES microgrid, a model for each main subsystem (Photovoltaic, Wind Generator, Accumulator, Fuel Cell, Electrolyzer, Hydrogen Storage Tank and Compressor) is developed in MATLAB environment.

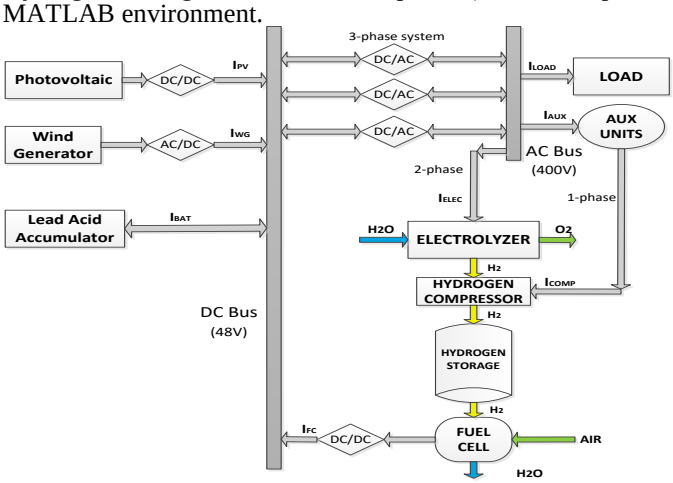

Figure 1 Microgrid topology and subsystems

A. Photovoltaic system

The model that is used is the one-diode model and is referred in subsystems with specific number of cells in series. The relationship between current and voltage is given by [1]:

$$I_{pv} = I_L - I_D - I_{ch} = I_L - I_o \cdot \left[\exp\left(\frac{V_{pv} + I_{pv} \cdot R_s}{\alpha} \right) - 1 \right] - \frac{V_{pv} + I_{pv} \cdot R_s}{R_{sh}} \quad (1)$$

The output power from the PV array is given by:

$$P_{pv} = V_{pv} \cdot I_{pv} \cdot \eta_{conv} \quad (2)$$

where η_{conv} is the efficiency of a DC/DC converter (~90-95%).

B. Wind generators

The model is based on the characteristics of the power of turbine at steady state and is given by: [2]

$$P_w = c_p(\lambda, \beta) \cdot \frac{\rho A_w}{2} \cdot v_{wind}^3 \cdot \eta_{conv} \quad (3)$$

where η_{conv} is the efficiency of a AC/DC converter (~90-95%).

C. Lead-acid accumulator

The KiBaM model [3] is used to describe the dynamics of the accumulator. It requires a current as input (positive for discharging and negative for charging) and calculates the voltage and the SoC (State of Charge) of the accumulator. The SOC is the fraction of the current capacity of the accumulator at each time instant, divided by its nominal capacity.

D. *Proton exchange membrane electrolyzer*

The voltage-current characteristics of the PEM electrolyzer are taking under consideration the overvoltages that occur at the electrodes and the ohmic resistance. The following equation describes the voltage-current characteristics [1]:

$$V_{elec} = V_{rev,elec} + \frac{r_1 + r_2 \cdot T_{elec}}{A_{elec}} \cdot I_{elec} + \left(s_1 + s_2 \cdot T_{elec} + s_3 \cdot T_{elec}^2\right) \cdot \log\left(\frac{t_1 + t_2 / T_{elec} + t_3 / T_{elec}^2}{A_{elec}} \cdot I_{elec} + 1\right) \quad (4)$$

The production rate of hydrogen in an electrolyzer is given by the Faraday's Law [4]:

$$\dot{n}_{H_2} = \eta_F \cdot \frac{n_c \cdot I_{elec}}{n_e \cdot F} \quad (5)$$

E. *Proton exchange membrane fuel cell*

As in PEM electrolyzer the activation overvoltage, the ohmic losses and also mass transport limitations are considered in the voltage-current relationship of the PEM fuel cell which is given by the following equation [1, 4]:

$$V_{fc} = E - \eta_{act} - \eta_{ohmic} \quad (6)$$

The hydrogen consumption rate in a PEM fuel cell is similar to the PEM electrolyzer (eq.5)

F. *Hydrogen storage tanks*

The equation that describe the pressure inside the storage tank is given by Wan der Waals Law and is as follows [1]:

$$P_T = \frac{n \cdot R \cdot T_{stor}}{V_T - n \cdot b} - \alpha \cdot \frac{n^2}{V_T^2} \quad (7)$$

G. *Compressor*

The polytropic work from the compressor as well as the actual energy demand for the motor operation is given by [1]:

$$\Delta W_{pol} = \frac{\kappa}{\kappa - 1} \cdot n_{H_2,comp} \cdot R \cdot T_I \cdot \left[\left(\frac{P_2}{P_1}\right)^{\frac{\kappa-1}{\kappa}} - 1\right] \Big/ \eta_{comp} \quad (8)$$

III. ENERGY MANAGEMENT STRATEGY

The following flowchart depicts the energy management strategy that was applied to the power system.

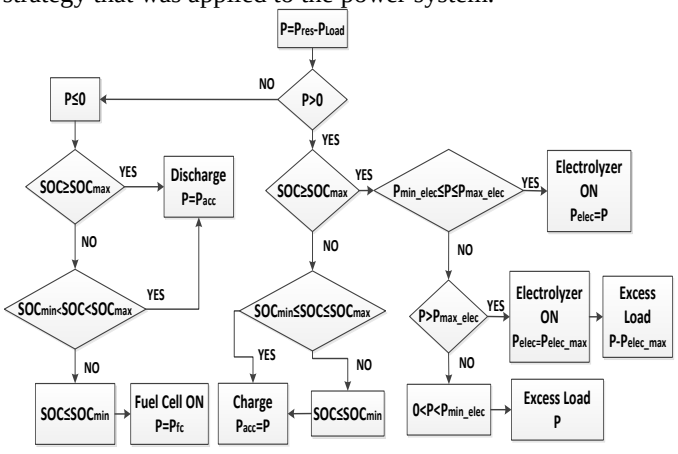

Figure 2 Energy management strategy for the autonomous microgrid

The main objective for the applied EMS is the satisfaction of the load requirements [4, 5]. Any energy surplus is stored with priority to the accumulator and then in the form of hydrogen through the electrolyzer due to constraints and lifespan of the later. Likewise any power shortage is first met from the accumulator and then from the PEM fuel cell according to SOC limitations given to the former.

IV. RESULTS ANALYSIS OF THE OPERATION

In order to evaluate the EMS a simulation of a day period with a step of 5 minutes was performed. For the PV system and WG real solar irradiation and wind speed data was used so as for the applied load demand.

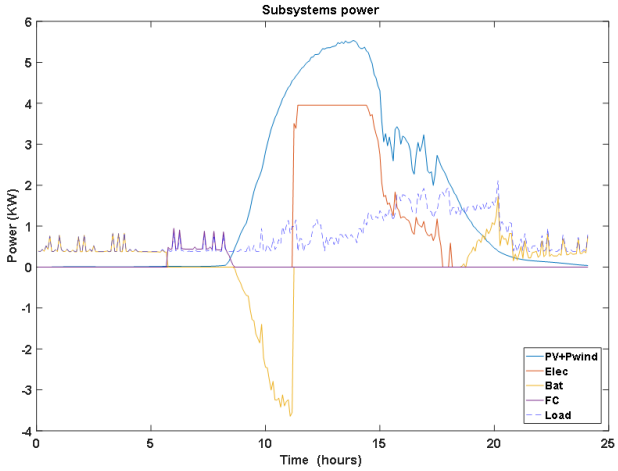

Figure 3 Power distribution on the systems

It is concluded from Figure 3 that with the applied energy management strategy not only the load demand is met but also the constraints for the functionality of the sensitive devices are fulfilled. In cases of power surplus and after the battery is charged, the electrolyzer stores the excess energy in form of hydrogen. In cases of energy shortage the fuel cell provides power to meet the load demand after the accumulator discharged and reached the minimum defined state of charge.

V. FUTURE WORK

As future work, a model predictive approach will be implemented combined with an optimization-based EMS for autonomous microgrids with the utilization of a Finite State Machine and propositional logic approach.

REFERENCES

[1] Ø. Ulleberg, "Stand-alone power systems for the future: optimal design, operation & control of solar-hydrogen energy systems," PhD thesis. Norwegian University of Science and Technology, 1998.
[2] Siegfried H. "Grid integration of wind energy conversion systems. "John Wiley & Sons Ltd, 1998.
[3] Manwell JF, McGowan JG. "Lead acid battery storage model for hybrid energy systems. " Solar Energy, 1993;50:399-405.
[4] Larminie J, Dicks A. "Fuel cell systems explained. " 2nd ed. John Wiley & Sons Ltd, 2003.
[4] Ipsakis D, Voutetakis S, Seferlis P, Stergiopoulos F, Elmasides C. "Power management strategies for a stand-alone power system using renewable energy sources and hydrogen storage. " International Journal of Hydrogen Energy, 2006;34(16):7081e95.
[5] Ziogou C, Ipsakis D, Elmasides C, Stergiopoulos F, Papadopoulou S, Seferlis P, Voutetakis S. "Automation infrastructure and operation control in a stand-alone power system based on renewable energy sources. " Journal of Power Sources, 196(2011): 9488-9499.

System Identification and Model Order Reduction of a Li-ion Battery and Ultracapacitor Forklift

P. Kakoulidou[1], C. Ziogou[2], C. Yfoulis[1], S. Voutetakis[2], S. Papadopoulou[1]

(1) Department of Automation Engineering, Alexander Technological Educational Institute of Thessaloniki, Thessaloniki, Greece

(2) Chemical Process and Energy Resources Institute (CPERI), Centre for Research and Technology Hellas (CERTH), Thessaloniki, Greece

***Abstract*—The purpose of this work is to apply system identification and model order reduction techniques in order to derive reliable mathematical models for a hybrid fuel cell – battery-ultracapacitor forklift vehicle. The system under consideration comprises of a Li-ion battery and an ultracapacitor (UC) as a first approach. The mathematical models that are created with system identification methods will be used for the optimal energy distribution for various driving cycles.**

I. INTRODUCTION

Electric forklifts are widely used in a wide variety of companies and serve multiple tasks in their shifts. A fuel cell powered forklift is equipped with a Polymer Electrolyte Membrane (PEM) fuel cell, a lithium ion (li-ion) battery and an ultracapacitor. The energy distribution among these subsystems is controlled by appropriate energy management strategies that ensure the optimum response of the forklift.

II. SYSTEM MODEL

In order to study the behavior of the forklift, two models for its subsystems, battery and ultracapacitor, were developed in MATLAB environment.

A. Li-Ion Battery

The battery model was determined using experimental data from a li-ion battery from a forklift with a sampling time of 60s. The system identification method was applied using these data in Matlab environment, in order to create a mathematical model to describe the relationship between input (current) and output (voltage) of the battery. Table I shows the li-ion battery's specifications per cell [3].

TABLE I
BATTERY MODEL SPECIFICATIONS

Model Name	LFP700AHA, 630-700 Ah
Nominal Voltage	3.2 V
Capacity	700 Ah
Operating Voltage	Max 3.8 V-Min 2.8 V
Deep Discharge Voltage	2.5 V
Maximal Charge Voltage	4 V
Optimal Discharge Current	<350 A
Maximal Discharge Current	<2100 A
Max Peak Discharge Current	<7000 A
Optimal Charge Current	<350 A
Maximal Charge Current	<2100 A
Maximal Continuous Operating Temperature	65°C

Figure 1 shows the voltage of the battery (V_{bat}) and the respective current (I_{bat}). The experimental data include 13 discharging and 12 charging data sets, that correspond to a battery cycle. The way this battery behaves during charging is called equalization charging. The 16th order of the original system can be justified as the system behaves like an integrator with multiplicity 16 at charging periods.

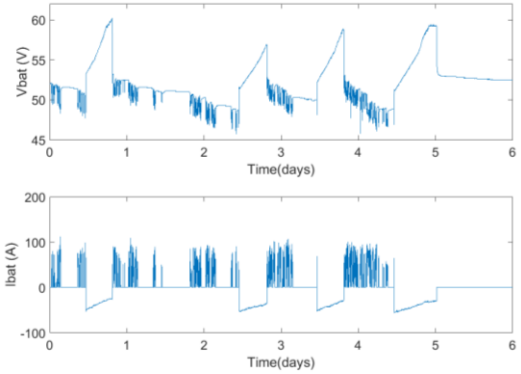

Figure 1.Experimental data from li-ion battery used in electric forklift

The equalization charging occurs after normal charging is complete and it is caused due to the fact that a battery stack may have fairly matched cells. Over time, the cell matching degrades due to charge/discharge cycles, elevated temperature and general aging. An aged battery cell will charge and discharge faster than stronger or higher capacity cells and thus it becomes the limiting factor in the run-time of a system. Cells which have been charged first create this pattern by their output signal as they try to reduce their voltage in order for the other cells to be charged as well.

The model is a hybrid continuous time, transfer function which has 89.34% fit for charging data and 87.32% fit for discharging data. There were created two models to describe this battery. The first one describes equalization charging (I_{bat} <0) and the other the discharging (I_{bat} >0) of the system.
Equalization charging model is a 16th order model. Model reduction methods were used to reduce system's order for creating faster and easier calculation algorithms while controlling the whole system. The equalization charging model reduced via MDC (matched DC gain) method state-space model is:

$$A=\begin{pmatrix} -8.576e\text{-}15 & 0 & 0 \\ 0 & -2.562e\text{-}07 & -0.001155 \\ 0 & 0.001155 & -2.499e\text{-}06 \end{pmatrix} \quad B=\begin{pmatrix} -0.01264 \\ -0.002149 \\ 0.006707 \end{pmatrix}$$

$$C=\begin{pmatrix} 0.007092 & -0.002149 & -0.006707 \end{pmatrix} \quad D=\begin{pmatrix} 0.4025 \end{pmatrix} \qquad (1)$$

The transfer function of the equalization charging model reduced via MDC method is:

$$Y(s)=\frac{0.4025s^3-0.0001289s^2+5.695e-07s-1.195e-10}{s^3+2.755e-06s^2+1.333e-06s+1.143e-20} \quad (2)$$

The discharging state-space model is:

$$A=\begin{pmatrix}-0.0019 & -0.0000\\ 0.0000 & 0\end{pmatrix} B=\begin{pmatrix}0.0156\\ 0\end{pmatrix}$$

$$C=\begin{pmatrix}-0.0012 & -0.0162\end{pmatrix} D=\begin{pmatrix}-0.0266\end{pmatrix} \quad (3)$$

The transfer function of the discharging model is:

$$Y(s)=\frac{-0.02663s^2-6.986e-05s-3.867e-09}{s^2+0.001931s+3.625e-10} \quad (4)$$

The aforementioned models are observable and controllable. The SOC (State Of Charge) model was created using the Coulomb method, which means that SOC was calculated taking as variable the battery's current.

The battery SOC is calculated by[1,2]:

$$SOC(t)=SOC(t-1)+a\cdot\frac{\int Iin(t)\,dt}{C\max} \quad (5)$$

where 'a 'was determined as a semi-empirical constant parameter and Cmax=630 Ah. The battery's SOC changes between 20-100% around during the charging and discharging based on the experimental data. Figure 2 shows the model's response to forklift battery's experimental data.

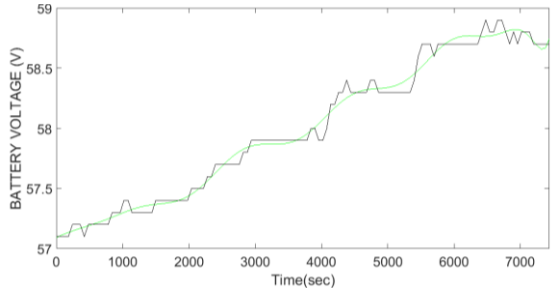

Figure 2. Li-ion battery model response during equalization charging

B. Ultracapacitor (UC)

The UC's model was created in a similar manner, as Li-ion battery's model, using experimental data with sample time equal to 1s and system identification. The UC's experimental data were taken from [4]. Table II shows the specifications of a UC BCAP3000 by Maxwell Technologies according to its datasheet [6].

TABLE II
ULTRACAPACITOR MODEL SPECIFICATIONS

Model Name	BCAP3000
Rated Voltage	2.7 V
Minimum Capacitance, initial, rated value	3000 F
Maximum Capacitance, initial	3600 F
Maximum ESR_DC, initial, rated value	0.29 mΩ

Figure 3 demonstrates UC's experimental results under UDDS (Urban Dynamometer Drive Schedule) driving cycle. The UC model response was validated in comparison to literature data as well [5].

Model equations in state-space form:

$$A=\begin{pmatrix}-96.1393 & -0.0792 & -0.0003\\ 0.1250 & 0 & 0\\ 0 & 0.0005 & 0\end{pmatrix} B=\begin{pmatrix}1\\ 0\\ 0\end{pmatrix} C=\begin{pmatrix}-0.1184 & -0.3397 & -0.4371\end{pmatrix} D=\begin{pmatrix}-0.0029\end{pmatrix} \quad (6)$$

The transfer function of the ultracapacitor model is:

$$Y(s)=\frac{-0.002889s^3-0.3961s^2-0.04249s-2.668e-05}{s^3+96.14s^2+0.009899s+1.926e-08} \quad (7)$$

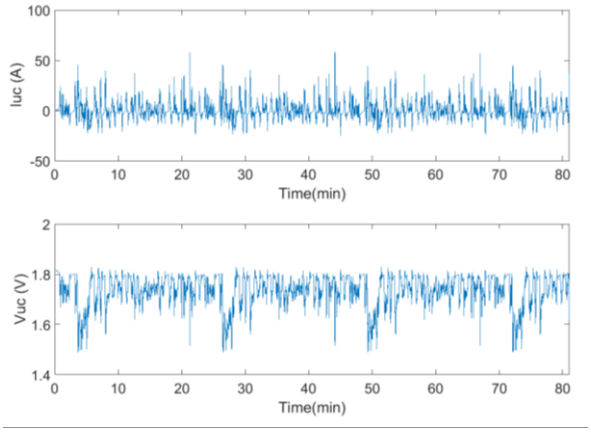

Figure 3.Experimental data under UDDS driving cycle

The model has 85.4% fit to experimental data. Fig. 5 shows the voltage difference against the experimental data which doesn't exceed 0.25 V with an average absolute error of 6%.

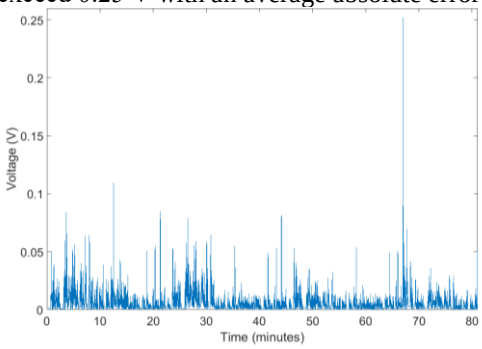

Figure 4.Absolute error between transfer function and experimental data

III. CONCLUSION

Overall the identified models show a very good response with respect to the experimental data and can be reliably used and resemble the dynamic behavior of the actual forklift's subsystems. The future work aims at the identification of a 10 kW PEMFC (Proton Exchange Membrane Fuel Cell) and design of an MPC (Model Predictive Control) control strategy including the identified subsystems of the entire forklift.

REFERENCES

[1] M. Bahramipanah, D. Torregrossa, R. Cherkaoui, M. Paolone , «Enhanced Electrical Model of Lithium-Based Batteries Accounting the Charge Redistribution Effect», 18th Power Systems Computation Conference

[2] B. Belvedere, M. Bianchi, A. Borghetti, «A Microcontroller-Based Power Management System for Standalone Microgrids With Hybrid Power Supply»,IEEE Trans.Sustain. ENERGY, vol.3, no.3,pp 422-431,2012

[3] http://liionbms.com/php/cells.php (accessed Nov 2017)

[4] Y. Wang, C. Liu, R. Pan, Z. Chen, «Experimental data of lithium-ion battery and ultracapacitor under DST and UDDS profiles at room temperature», 12, 2017, pp. 161-163

[5] L.Gauchia, A.Bouscayrol, J.Sanz, R.Trigui, P.Barrade, «Fuel Cell, Battery and Supercapacitor Hybrid System for Electric Vehicle: Modeling and Control via Energetic Macroscopic Representation», Vehicle Power and Propulsion Conference (VPPC), 2011 IEEE

[6] http://www.maxwell.com (accessed Nov 2017)

Smart Home Automation-Control and Monitoring System Using Microcontroller and Android Phone

Themistoklis Kolias, Konstantinos Kamoutsis, Evaggelos V. Hatzikos

Department of Automation Engineering, ATEI Thessaloniki

***Abstract*—This paper presents the design and implementation of a Smart Home model that aims for the resident's comfort, security, and reducing energy consumption. The system combines sensors and appliances activators to respectively get information from and control the house environment. As a primary controller, we used an Arduino Mega microcontroller. Furthermore, an Arduino Uno is used as secondary controller. Both communicate with an Android mobile application. Among Arduino's advantages, is the capability to control and monitor the system with low cost. Another one is its flexibility since its features can vary upon the resident's demands.**

***Index Terms*—Smart Home, Android device, Smartphone, Bluetooth, Arduino**

I. Introduction

SMART Home is the integration of technology and services through home networking for a better quality of living; it is a house that involves advanced automatic systems such as lighting, heating, and security. Smart home can provide remote control and monitor through a smartphone [1].

The Smart Home Model presented in this paper consisted of various subsystems to control and monitor the home with an Android application. The first one refers to the security system with a PIR sensor, gas sensor, sound sensor, and limit switches. The second subsystem is about the control of lighting and electrical devices. The third includes temperature sensor, LCD screen and a RTC (real time clock). Finally, there are plenty scenarios for the resident's comfort, protecting the home and also minimizing energy consumption. The main computer that controls and supervises the whole system is an Arduino Mega2560. An Arduino UNO is also used to reduce the workload of main controller [2]. The contribution of this project is the efficient interconnection of various tools to control and monitor a house.

II. Connectivity

To enable connectivity on the microcontroller, a Bluetooth device is used (Bluetooth module HC-05). This module is based on the CSR BC417 2.4 GHz Bluetooth Radio chip. The HC-05 series can act as master or slave. It has two modes, the command mode and the data mode. The Android based mobile application communicates with the microcontroller via the Bluetooth device [3].

A. Arduino

Arduino is an open-source design platform and easy-to-use hardware and software to create electronic projects. The microcontroller boards that are used on this project are the Arduino Mega 2560 and Arduino UNO, which are based on the ATmega2560 and ATmega328P respectively.

TABLE I
ARDUINO MEGA 2560 AND ARDUINO UNO SPECIFICATIONS

Microcontroller	ATmega328P	ATmega2560
Operating Voltage	5V	5V
Input Voltage	6-20V	6-20V
Digital I/O Pins	14 (6 PWM)	54 (15 PWM)
Analog Input Pins	6	16
DC per I/O Pin	20 mA	20 mA
DC for 3.3V Pin	50 mA	50 mA
Flash Memory	32 KB	256 KB
Clock Speed	16 MHz	16 MHz

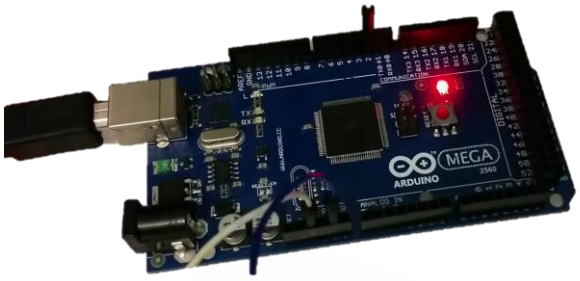

Fig. 1. Image of Arduino Mega 2560

Fig. 2. Image of Arduino UNO

B. Android application

The android application was designed using the MIT App-Inventor Integrated Development Environment (IDE) [4]. Bluetooth device allows android phone to communicate with the microcontroller effectively and efficiently. The application allows the user to control devices and monitor conditions in the home.

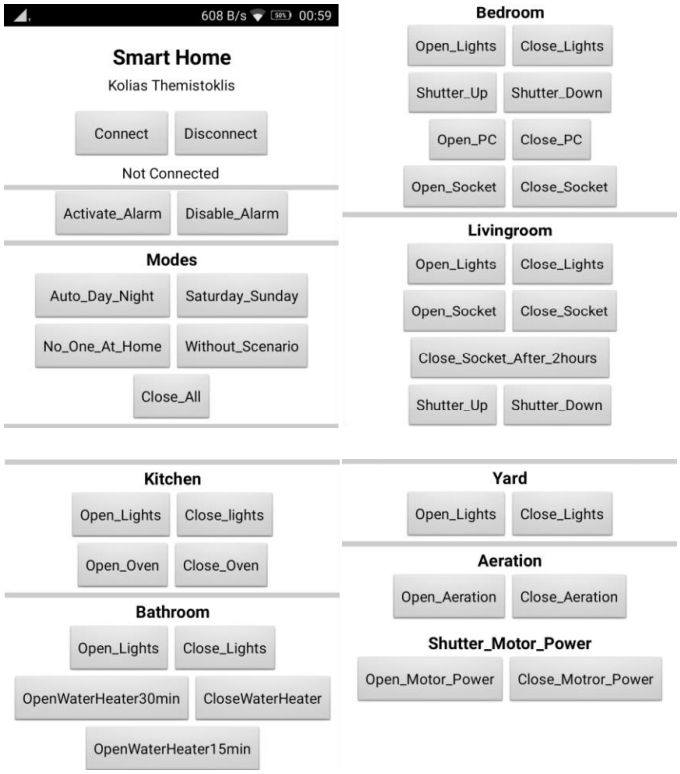

Fig. 3. Image of Android application

III. Applications

The developed applications [5] of Smart Home and security system are the following:

- Gas sensor detects gas leaks or fire and enables the alarm.
- PIR sensor detects movement in the place and enables the alarm.
- Security lighting operated by photocell.
- Limit switch installed on the door. The alarm is activated as soon as the door opens.
- Inside door opens automatically when a PIR sensor detects movement.
- Control of indoor air system (ventilation).
- Shutters open or close automatically depending on the temperature sensor which shows home's temperature on the application.
- Garden lights. A photoresistor turns on the garden lights during night and turns off during the day.
- Soft buttons on the android applications are used to turn on and off PC, lights, kitchen, and heater.
- System information on LCD.

The most important applications are the scenarios. "Auto Day Night" scenario enables water heater every morning and an alarm clock sounds to wake up the owner. When owner leaves the house, security alarm is enabled and ventilation works for two hours. When owner returns, the scenario enables security alarm and turns on the kitchen. Security lights and alarm are enabled at night [6]. Also, if any electrical device is turned on after a certain time limit, it is disabled automatically. "Saturday-Sunday" is almost the same, but different time schedule. "No One At Home" turns off everything and enables the security alarm. "Close All" scenario closes all the applications at any time [7].

Fig. 4. Model Design (front)

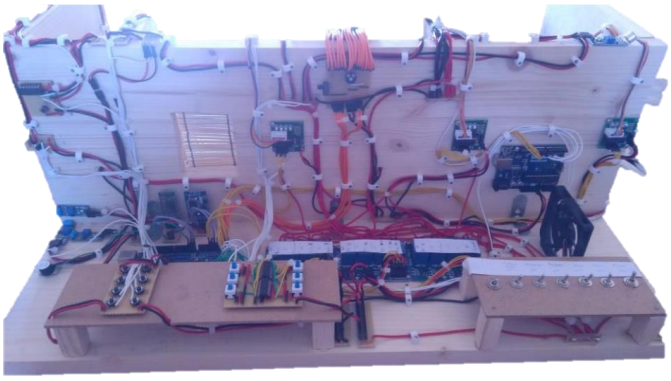

Fig. 5. Model Design (back)

IV. Acknowledgement

We would like to thank our supervisor Dr. E. Hatzikos for his cooperation and support throughout the various stages of project development. This project is part of the research programme developed between the Department of Automation Engineering, ATEI Thessaloniki and Kafkas Company for Home Automation.

References

[1] Vendela Redriksson, "What is a Smart Home or Building", (2011) April, Available at: http://searchciomidmarket.techtarget.com/definition/smart-home-or-building, Accessed: November 2017.
[2] Molly Edmonds, "How Smart Homes Work - Setting Up a Smart Home", (2011), Available at: http://home.howstuffworks.com/smart-home.htm, Accessed: November 2017
[3] Al-Qutayri, M.A., Jeedella, J.S.: Integrated Wireless Technologies for Smart Homes Applications. In Smart Home Systems, M. A. Al-Qutayri, Ed., ed: InTech (2010)
[4] http://www.appinventor.org
[5] Rosslin John Robles and Tai-hoon Kim, Applications, Systems and Methods in Smart Home Technology: A Review, International Journal of Advanced Science and Technology, Vol. 15, (2010) February, pp. 37-48.
[6] P Pavan Kumar, G Tirumala Vasu, "Home Automation & Security System Using Arduino Android ADK", *IJETER*, vol. 3, no.6, pp 190-194, 2015
[7] Mohamed Abd El-Latif Mowad, Ahmed Fathy, Ahmed Hafez, "Smart Home Automated Control System Using Android Application and Microcontroller", *IJSER*, vol. 5, Issue 5, pp 935-939, 2014

Fault Detection Voltage and Current Measurements Comparative Study

Kyriaki G. Eleftheriadou, Panagiota A. Mpirta, Dimitrios K. Papakostas

Department of Electronic Engineering T.E.
Alexander Technological & Educational Institute of Thessaloniki
Thessaloniki, Greece

***Abstract*—This paper presents a method to compare fault detection probabilities for both destructive and non-destructive failures using voltage and current measurements of circuits under test. Different input stimulus signals are applied in order to observe fluctuations in the examined measurements through Pspice simulations. The method differentiates due to the incorporation of different signal inputs according to the needs and the specifications of each circuit. Experimental results are presented showing the effectiveness of the proposed testing method.**

***Index Terms*— Analog circuits, Testing, Fault detection.**

I. INTRODUCTION

Fault diagnosis is a particular branch of circuit theory and is directly related to methods and techniques for detecting and isolating faults [1-6]. There are many factors that can affect the proper operation of a circuit and for this reason it is difficult to control the process. It is worth noting that the accuracy and efficiency of test methods for generating, analyzing and, by extension, manufacturing (practical piece of) electronic circuits, for this reason a good method must be able to detect all circuits exhibiting a defect before they are used [3]. In the following in the first section the fault models are presented while in the second section the method of detection fault is presented. The analysis of the results of the method follows and finally conclusions have been remarked.

II. FAULT MODELS

A damage is a constructional fault in the circuit or a problem in some element of the circuit which may lead to a possible failure. In order to predict the behavior of the circuit, it is necessary to find a realistic fault model with which their behavior can be approached. The fault list is the set of all faults that are modeled and the test method must be capable of detecting all of these faults. At this point, it should be clarified that overall traceability of faults does not mean that all the faults are detected, but only those that can be approached by the particular model. Realistic analog fault models can be extracted having knowledge of circuit behavior [6], which may be one of below:

1. Catastrophic Failure: Circuit is not at all operational.
2. Unacceptable performance degradation: In this case, the circuit still works but some feature is not within specifications.

The faults of the analog circuit are categorized as follows:

- Destructive (catastrophic) Faults are all the errors that can cause a catastrophic failure in the circuit, such as open circuits, short circuits, and very large changes in their circuit parameters.
- Non-destructive faults (parametric) are those that can lead a circuit to an unacceptable performance degradation. These faults result in the variations of characteristics in the manufacturing process. These errors include changes in circuit parameters higher than the tolerance limits.

More specifically, the fault models used are the short circuit which was applied with the help of a 10Ω resistance and the open circuit for which a 10MΩ resistance was used (destructive faults) [1,2,4]. For non-destructive faults the value of each resistance was changed, transforming it by ±25% of its original value and also by ±50% deviation.

III. FAULT DETECTION METHOD

The proposed method is based on a simplification of similar used methods [1,2,5]. A step-by-step approach of the method is shown in the flow chart of figure 1. Initially, the correct (non-faulty) circuit for all different input stimulus is simulated. Next, the tolerance limit is set between 5% and 25% with a 5% step for each applied measurement. Then all the faulty cases are simulated one by one, and if the resulting measurement values are within the tolerance limits, then this faulty case is to be considered as non-faulty, otherwise when the resulting measurement values are outside the tolerance limits it has to be considered as false. At the end of the diagram there is the IF command which separates the correct ones from the incorrect detections, helping to calculate the fault probability percentages rates of each measurement. For example, for a non-faulty measurement of 5V and a tolerance limit of 10%, if the resulting measurement of the examined circuit is between 4.5V and 5.5V then this circuit is considered as non-faulty, while otherwise in considered as faulty, examined using only this specific measurement.

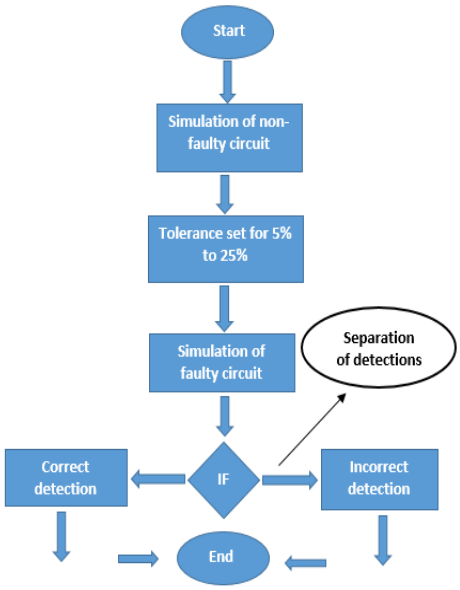

Fig. 1. The flow chart of the method.

IV. Results

The results of two circuits (a typical one stage and a typical two stage common emitter amplifiers) were examined [3]. Three different input signals were applied, namely a sinusoidal signal (SIN), a square pulse (PULSE) and a saw-pulse (PR). The frequency was set always at 1KHz while there were some fluctuations on the pulse width depending on the different input signals which were used. In the first circuit the width for sinusoidal input was 0.25Volt, for square input signal 0.5Volt as the same value of 0.5Volt exists for the saw input signal. In the second circuit the width for sinusoidal input was 0.05V and for the other two signal cases input 0.1V.

In each circuit separately, the examined measurements are the output voltage (Vout), the output current (Iout) and the positive power supply current (I+), with their respective peak to peak (p-p), rms and first harmonic values. Additionally, in each circuit separately, the two types of faulty cases (destructive and non-destructive) were applied. The set of faults that was applied in the one stage amplifier involved 54 faults (26 destructive and 28 non-destructive) while in the two stage amplifier 94 faults (46 destructive and 48 non-destructive) were applied.

In the case of catastrophic failures, sinusoidal input always gives higher error detection rates close to 95%. The saw and the square pulse exhibit lower rates near 90%. In contrast, in the case of non-destructive damage, the square input signal is the one that displays higher rates close to 65%. Turning to sinusoidal input gives lower percentages between 55% and 60% and last comes the sinusoidal signal with 45% to 50%.

The results shown that in the case of destructive faults the sinusoidal input signal results in higher fault detection rates. Even in the case of non-destructive faults, saw and square pulse result in higher fault detection rates, leaving the sinusoidal signal in the last position. Finally, it is worth noting that the Iout measurements with its rms and first harmonic values offer greater detection traceability.

In figure 2 and 3, the stages coupling capacitor C3 short-circuit fault (C3S) of the two stage amplifier circuit is shown.

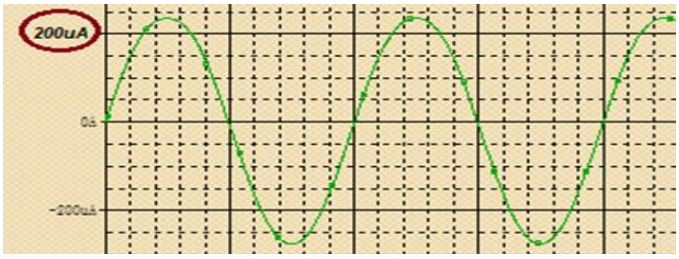

Fig. 2. Output Current Waveform of the non-faulty circuit.

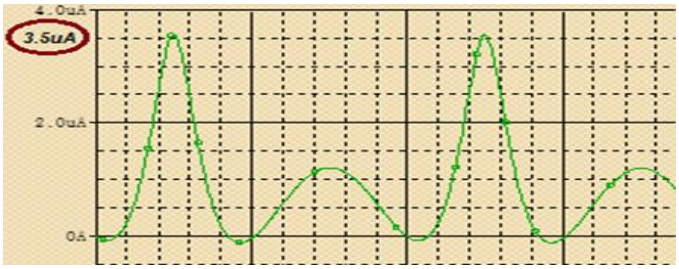

Fig. 3. Output Current Waveform of the C3S faulty case.

The waveform of the non-faulty operation of the circuit varies considerably from that resulting from the application of the faulty one. The output current waveform of the correct operation of the circuit has a maximum value of 200uA whereas in the case of failure it reaches only 3.5uA. This failure is easily detected by the method chosen as there is a large deviation of the resulting values.

V. Conclusions

Comparison of fault detection probabilities for both destructive and non-destructive failures using voltage and current measurements of circuits under test is studied. Different input stimulus signals were applied in order to observe fluctuations in the examined measurements through Pspice simulations. The advantage of the method is the simplicity effectiveness using only one measurement.

Concerning the examined circuit cases, it is observed that the output current Iout, with its rms and first harmonic values offer greater detection traceability. Also, comparative results from three different input stimulus, show that the non-linear (pulse or saw) input stimulus always gives larger fault detectability values than the linear sinusoidal signals, since for destructive faults sinusoidal input always results to higher detection rates.

References

[1] Papakostas D.K., Hatzopoulos A.A., "Supply current testing in linear bipolar ICs", IEE Electronics Letters, Vol. 30, No. 2, pp 128-130, January 1994.
[2] Papakostas D.K., Hatzopoulos A.A., "Fault detection in linear bipolar ICs: comparative results between power supply current and output voltage measurements", Proc. IEEE Int. Symp. on Circuits & Systems, ISCAS 94, vol. 5, pp 61-64, London, May 1994.
[3] A. Malvino, D.. Bates, "Electronic Principles", 7th. Ed, 2013, pp. 372-4.
[4] Pouros S.P., Vassios B.D., Papakostas D.K., Hatzopoulos A.A. “Input Stimulus comparison using an Adaptive FPGA-based Testing System”, 2014 IEEE Int. Symp. on Circuits & Systems, ISCAS 2014, pp. 277-280, Melbourne, Australia, June 1-5, 2014.
[5] R. Mozuelos, Y. Lechuga, M. Martizen, S. Bracho, "Structural Test Approach for Embedded Analog Circuits Based on a Built-in Current Sensor", March 2011, pp. 183-189.
[6] A. D. Spyronasios, "Analog and Mixed Circuit Testing Method", Phd Dissertation, Thessaloniki, March 2012, pp 7-10.

Embedded Infrared Monitoring System

Filippos Bazakas
filipbazakas@yahoo.gr
Christos Avdimiotis
cs.avdimiotis@gmail.com
Athanasios Mekras
athmekr@gmail.com
Stylianos-Georgios
steliospaap@gmail.com
Leonidas Katselas
katselas@auth.gr
Alkis Hatzopoulos
alkis@eng.auth.gr

Aristotle Univ. of Thessaloniki

University Campus
54124 Thessaloniki
Greece

***Abstract*—With Internet Of Things becoming more and more popular in the current days, many building monitoring devices have come to the foreground. These devices very often require a complex wired supply-camera setup, which is associated with large scale devices and a high implementation cost. Moreover the cameras'resolution might be way too advanced when used for simple monitoring applications, such as people counter. This will lead to a very complex image processing algorithms and a high power consumption. Finally, since face recording cannot be legally allowed without permission, the usage of such devices can be forbidden. That means that each property owner needs to have a relevant acknowledgements when using such IOT monitoring devices.**

***Index terms*—** IOT, Infrared, Embedded, Monitoring

I. Introduction

In this work, a small sized Printed Circuit Board (PCB) is presented, which can surpass these difficulties. The whole system is based on the Panasonic's Infrared array sensor's readings, Grid-Eye. According to object's infrared radiation, this sensor can detect temperature variations in a distance of up to five meters. Moreover, it is unable to recognize human faces, respecting the human right for privacy.

The voltage regulator that was used (IRM03-xx), converts a common 220V electrical socket's supply to 3.3V, surpassing the need of a special supply setup. The low cost Atsamd21g18a microprocessor is a suitable choice for simple building monitoring applications. Finally, with the usage of the ESP12S transition module, signals can be sent utilizing a local Wi-Fi configuration.

The described system was placed inside a 5.4x5.3x3cm 3D-printed box and has been tested, under real circumstances, to count the number of people who enter or leave a building. The results showed that the system can work even under extreme conditions (e.g. many people entering and leaving the building the same time or when the person's temperature is very close to the environment's temperature).

II. Prior Work

Many techniques like the running Gaussian average or Kernel density estimation are proposed in 1. Each one comes with its own advantages in terms of 1) reliability, 2) adaptation to the changes of the environment, 3) algorithm complexity and 4) memory requirements. Also people tracking tracking techniques in low-quality images are presented in [2, 3].

III. Detection Algorithm

A. Input data

Grid-Eye generates an 8x8 float array of temperature in Celcius. To increase the difference between temperatures each cell is multiplied by a factor four. This array is used as input to our detection algorithm.

B. Noise reduction

To minimize the noise impact a self-conceived technique was used. Instead of receiving a single frame as input, we calculate the average temperature of each cell from three consecutive frames. More than 80% of the noise is cut off from and the "hot"object is depicted more efficiently . The equation for calculation of the input array is shown below:

$$Input(i) = \frac{F_k(i) + F_{k-1}(i) + F_{k-2}(i)}{3}, \tag{1}$$

where F_k is the current frame.

C. Background subtraction

Background subtraction is a necessity, in order to determine whether a "hot"value of a pixel depics a person who shifts in the tracking field or just a steadily hot object of the background. The method that was chosen was the simple median average of the first N frames for each of the 64 pixels. The number of the frames N was chosen initially as 15 but later changed to 11 due to some hardware complications. Equation 2 shows calculation of the background for the i_{th} pixel:

$$B(i) = \frac{\sum_{k=1}^{N} B_k(i)}{N}, \tag{2}$$

This method excels in criteria 3, 4, which was critical for our limited resources of our PCB. The drawback is that neither adapt to dynamic changes of the background, nor can offer reliability. The solution for these problems is the recalculation the background temperature.

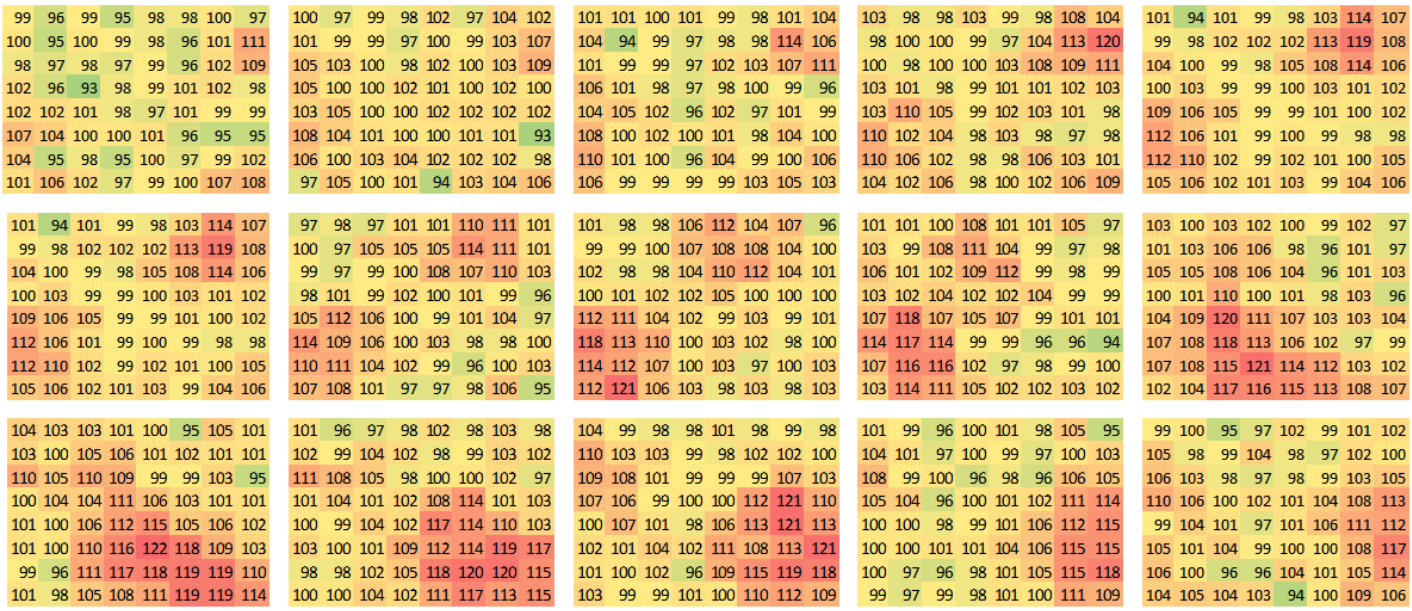

Fig. 1: An example of two humans entering-leaving a room.

D. Threshold subtraction

After the background subtraction, a second subtraction was implemented between each pixel and a threshold, in order to determine if the desired difference between the environment value and the current value is actually big enough to be characterized as “hot”.

First value of the threshold was 8, which corresponds to 2 Celsius degrees. Later, through noise cancelation was reduced to 5, i.e. 1.25 Celsius. Furthermore reduction of the threshold, in order to increase the sensitivity of the algorithm, is feasible.

E. Local Maxima

In order to pinpoint the coordinates of the local maxima points, we spot all the points that are greater than it’s 9 neighbor points. This method is feasible only for one scale images.

F. Blob-detection

Areas with higher temperature values (blobs) are being procceced, in order to clarify if the detected blob is a human. It is observed that extremely circular blobs can only occure under noise existance, therefore they are filtered out. After the first filter-phase, local maximum values are being searched, in order to clasify each of the blobs as a human passing in front of the sensor. Finally, the algorithm is able to decide whether there was any entrance or exit depend on various conditions.

IV. Experiment Results

The objective of our experiments is to show the effectiveness of our system. A Grid-Eye was placed at the entrance of a room to detect if a human enters or leaves. In our experiment a person enters the room from the left side and another out leaves from the right. This action is shown in 15 fromes in Fig1

V. Conclusion

The results were satisfying. With less than 8kB of memory and length code of only 500 lines, the algorithm was able to track faultless various simple and complicated conditions. Our system is tested successfully in places with single and multiple entrances and with unpredictable routes. Further improvements, would require to increase the complexity of the algorithm to be able to distinguish people from animals.

References

[1] M. Piccardi, “Background subtraction techniques: a review,” vol. 4, pp. 3099–3104, 2004, doi:10.1109/ICSMC.2004.1400815.

[2] M. Berger and A. Armitage, “Room occupancy measurement using low-resolution infrared cameras,” 2010, doi:10.1049/cp.2010.0521.

[3] S. Hinz, “Fast and subpixel precise blob detection and attribution,” in *Image Processing, 2005. ICIP 2005. IEEE International Conference on*, vol. 3. IEEE, 2005, pp. III–457, doi:10.1109/ICIP.2005.1530427.

Design and manufacture of voice distortion device in real time

Stefanos Giannopoulos, Maria Drakaki
Department of Automation Engineering, Alexander Technological Educational Institute of Thessaloniki, Thessaloniki, 57400, Greece

In this paper, entitled "Design and manufacturing of voice distortion device in real time" the manufacturing process of a device from design to final product has been implemented. The design of both the electronic part as long as their housing from A to Z without using finished components. The purpose of this is to reduce the cost of mass production. During this work there will be presented ultramodern manufacturing processes where available, as well as optimizations on the product and a financial analysis to produce copies in the best possible production time.

The part of electronic design and manufacturing, includes the process that drove the project from the idea into implementation. It all begun with a brief research on equivalent circuits, in order to decide the optimal technology that will be used in the end. The circuit is based on some functions of Operational Amplifiers in combination with a special purpose IC called PT2399. After a short period of tests on a test board, the final VERO board (1) was soldered, ready to deliver excellent sound quality to the user. In the end, the circuit has been designed in a PCB design software.

The manufacturing process of housing, went from the first sketch to G code through the use of cutting edge of technology CAD CAM and Illustration software packages. The result was released after consideration of the needs for protection of electronics, as well as optimal human machine interface.

After some tests in laboratory and real music studio, there is a detailed explanation for different assets that can be adapted to make the product more viable in the market. Last but not least there is a financial analysis of the costs required to produce this product.

1. Product

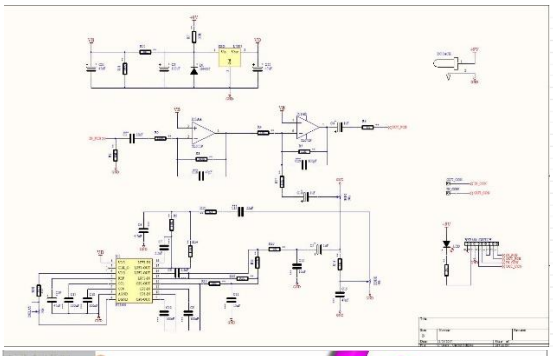

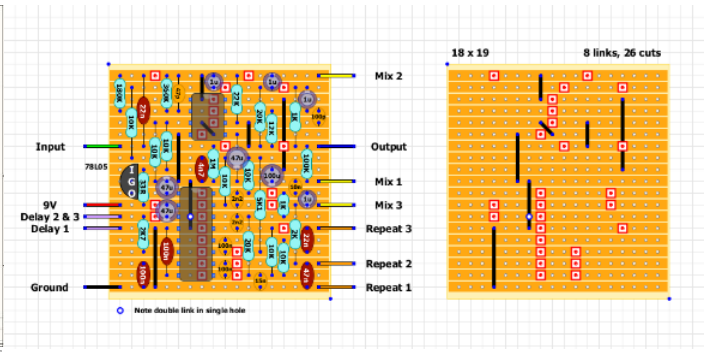

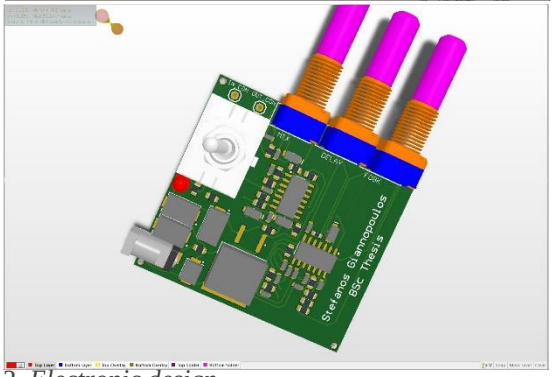

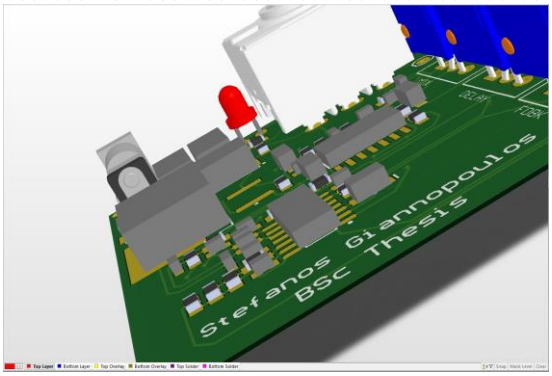

2. Electronic design

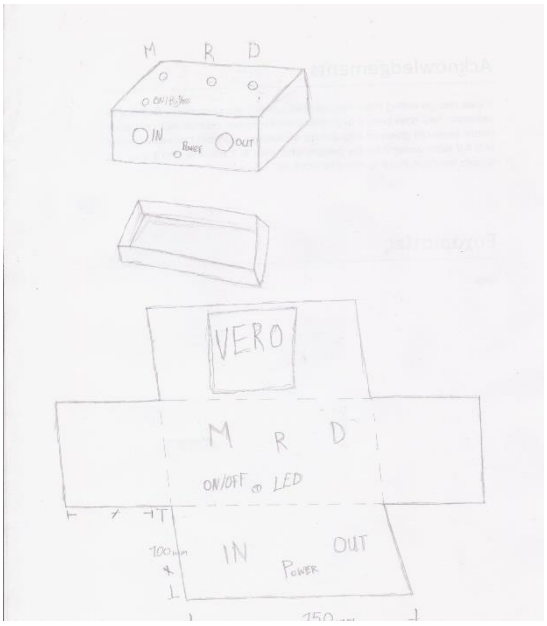

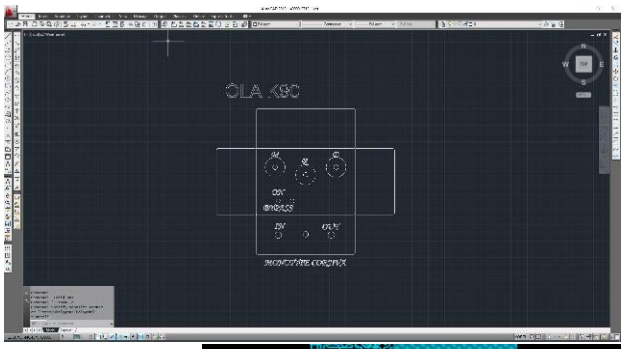

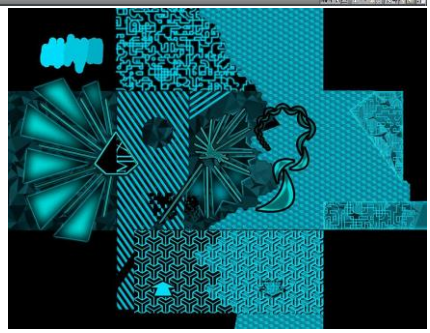

3. Mechanical design

*(1) Veroboard is a brand of stripboard, a pre-formed circuit board material of copper strips on an insulating bonded paper board (*https://en.wikipedia.org/wiki/Veroboard

Georgios Vlachogiannis[1], Panagiotis Kyriakidis-Tingilidis[1], Dimitrios Bechtsis[1]

Automation Engineering Department, Alexander Educational Institute of Thessaloniki

An Intelligent Autonomous Vehicle (IAV) prototype for industrial facilities

Abstract: One of the most evolving state-of-the-art technological solutions is the development of Intelligent Autonomous Vehicles (IAVs) that navigate in industrial facilities, monitor the industrial processes and make unattended real time decisions based on microelectronics and sensor technologies. IAVs use sophisticated protocols for communicating with each other and with all the entities in the industrial facility (equipment, software management systems e.t.c.). For our prototype we used a custom chassis with two separate geared motor-driven wheels controlled by encoders and a single caster wheel. The main data processing unit is a Raspberry Pi board with a standard Wifi shield and a PiFace digital 2 extension board with relays. Additionally, we included an L298N dual H-bridge to drive the motors, a camera for obstacle avoidance and identification of regions of interest; alongside with ultrasonic and infrared sensors. Moreover, we added sufficient cooling with a 12mm fan, an adjustable switching regulator for the electronics, and finally, a Lithium Polymer (LiPo) battery. The PiFace is a H.A.T. (Hardware Attached on Top) board, which is used with Raspberry Pi and consequently cuts off access to the original pins. In our case, we created a custom board, and attached the PiFace on top of it, releasing the majority of the pins for further use.

Furthermore, we developed a custom operating system (OS) for the Raspberry Pi, based on Ubuntu Linux and the Robot Operating System (ROS). ROS is an open-source, meta-operating system that provides hardware abstraction, low-level device control, data fusion and manipulation. Our vehicle can be remotely controlled using a camera and a custom ROS interface while on the same time identifying the surroundings of the facility layout with image recognition algorithms. The vehicle could autonomously navigate in an industrial facility and monitor real-time processes in order to provide decision makers with valuable feedback from the shop floor.

DC-Link Capacitor Voltage Balancing in a Three-Phase Neutral Point Clamped Inverter

Grigoris Sergentanis[1], Fotis Stergiopoulos[2] and Dimitrios Triantafyllidis[2]
[1] School of Electrical and Computer Engineering, Aristotle University of Thessaloniki,
[2] Department of Automation Engineering, Alexander Technological Educational Institute of Thessaloniki

***Abstract*—Multilevel inverters become increasingly important as the needs of power transfer and control rise. They can output ac voltages and currents with significantly lower harmonic distortion over the classic two-level inverters. This paper first presents the structure of a three-level neutral point clamped (NPC) inverter. Afterwards, it points out the voltage balancing capabilities of a simple to implement carrier based modulation strategy. It also achieves an average current of zero in the neutral point. This modulation is simple enough to be implemented in cheap microcontrollers and opens the way to usage of multilevel inverters in low power applications.**

***Index Terms*—voltage balancing, multilevel inverter, NPC inverter, SPWM**

I. Introduction

MULTILEVEL inverters are known to present several advantages especially for high power applications, operating at high voltages with an improved harmonic content over classical two-level inverters [1-5]. A Neutral Point Clamped (NPC) (Figures 1,2) inverter uses -clamping- diodes to connect to the neutral point. This increases the number of voltage levels that can be generated in a phase. It can use all the modulation techniques that are used in classical inverters. In this paper, a carrier based modulation is examined. Two carrier waves are used with the in-phase-disposition (IPD) technique. A voltage controller is needed to balance the capacitor voltages (Figures 1,2), otherwise the distortion in the voltage and current waveforms is increased. In this paper, the controller is based on offsetting the reference voltages based on the voltage difference of the capacitors, as well as the phase currents [1]. The reference voltages have been modified in order to obtain SVM patterns, which achieve maximum range of linear operation mode. The used offset is calculated from the equation below

$$v_{i_{off}} = -k_p|\Delta v_c| \cdot sign(\Delta v_c i_i) \cdot sign(v_{ip} - v_{in} - 1) \quad (1)$$

in which k_p is the controlled variable of the closed loop system, Δv_c the differential voltage of the two capacitors, i_i the corresponding phase current, v_{ip} and v_{in} are the modified voltages derived from the reference phase voltage, which are compared with the positive carrier and the negative respectively.

To implement the load, a three phase inductive load was added. Simulations were made using Matlab Simulink 8.7®, showing the potential this controller has for voltage stabilization.

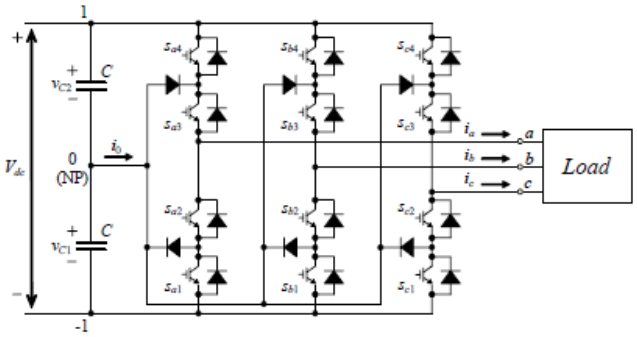

Fig. 1. Schematic of a three phase NPC inverter

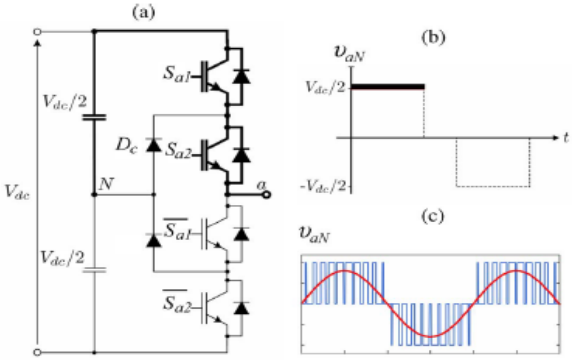

Fig. 2. Working principle of a three-level NPC inverter. (a) Conduction starts to generate a positive load voltage. (b) Positive load voltage. (c) Complete load voltage showing three levels.

II. CONTROLLER PARAMETERS AND RESULTS

Initially, a three-level NPC inverter was developed in Simulink suing a power supply of a 400V battery. Each capacitor should be always charged at half the voltage. However, initial voltages in the capacitors were deliberately set to 250V and 150V respectively, as to show the response time of the controller in case of a voltage imbalance. Several values were tried, and the results point out that at k=0.05, the response time is satisfactory, in the order of one period (20ms).

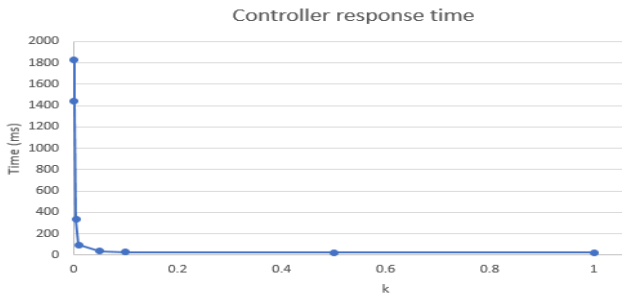

Fig. 3. Graph of the different settling times for the controller.

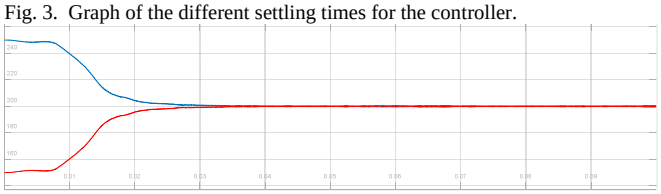

Fig. 4. Graph of the capacitor voltages at the inverter startup with 50ms time shown. It is shown that the settling time is around 30ms.

Using this value for k, a back-to- back (AC/DC/AC) system was also tested using a 400V, 50Hz three phase AC power source and a diode rectifier with 1mF capacitors, to test the performance of this modulation strategy in a realistic power distribution system. The results of the load voltage and current are satisfactory, as shown in the figures below. Capacitor voltages also appear in synchronization and the neutral point current average is zero.

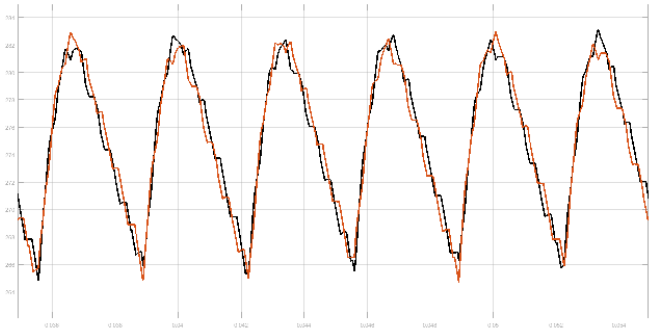

Fig. 5. DC-link capacitor voltages in the closed loop control of a back-to-back system.

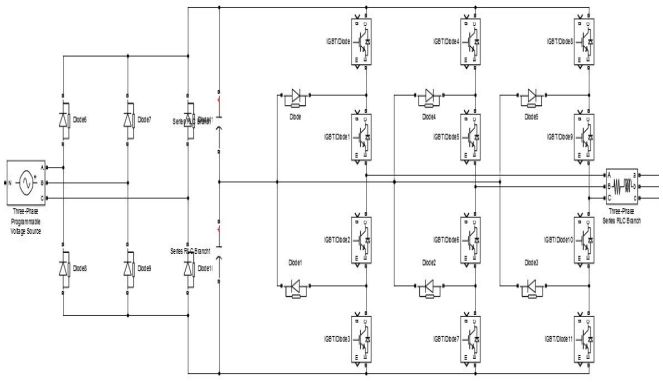

Fig. 6. Simulink model of an AC/DC/AC system

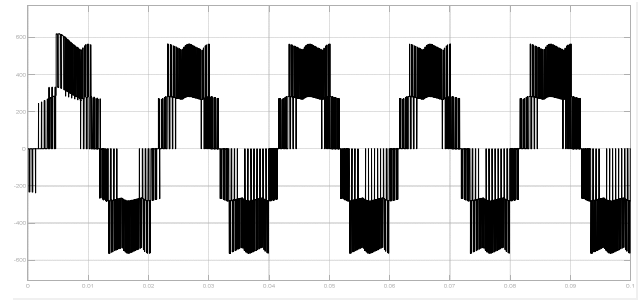

Fig. 7. Line to line voltage of the RL load.

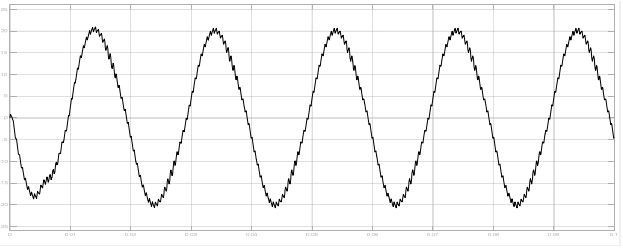

Fig. 8. Current of phase A of the RL load.

To evaluate how the closed loop control performs, the same simulation was performed in an open loop classical SPWM setting without voltage balancing. It was observed that the Total Harmonic Distortion (THD) without the voltage balancing technique was 4.10% and with the voltage balancing was 1.06%. Further work will examine other aspects of controller operation such as the effect of the switching frequency and examine the practical implementation of the scheme.

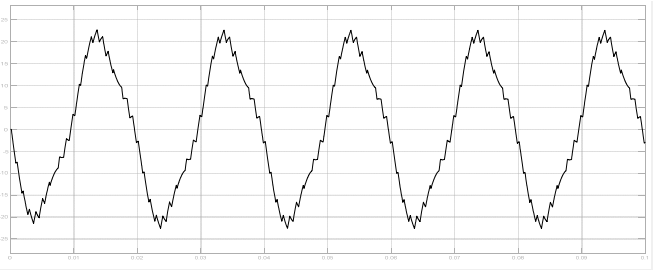

Fig. 9. Current of phase A of the RL load without voltage balancing.

REFERENCES

[1] J. Pou, P. Rodríguez, V. Sala, J. Zaragoza, R. Burgos, and D. Boroyevich, "Fast-Processing Modulation Strategy for the Neutral-Point-Clamped Converter with Total Elimination of the Low-Frequency Voltage Oscillations in the Neutral Point" IEEE Transactions on Industrial Electronics,vol 54, Issue: 4, Aug. 2007.

[2] J. Rodriguez, J.-S. Lai, and F. Z. Peng, "Multilevel inverters: A survey of topologies, controls, and applications," IEEE Trans. Ind. Electron.,vol. 49, no. 4, pp. 724–738, Aug. 2002.

[3] José Rodríguez, Steffen Bernet, Peter K. Steimer, and Ignacio E. Lizama "A Survey on Neutral-Point-Clamped Inverters," IEEE transactions on industrial electronics, vol. 57, no. 7, july 2010

[4] Brendan Peter McGrath, and Donald Grahame Holmes "Multicarrier PWM Strategies for Multilevel Inverters", IEEE transactions on industrial electronics, vol. 49, no. 4, august 2002

[5] Jih-Sheng Lai, and Fang Zheng Peng "Multilevel Converters-A New Breed of Power Converters", IEEE transactions on industry applications, vol. 32, no. 3, may/june 1996

Driving a Linear Sensor Array of Photodiodes with the use of AM3358 Sitara Processor

Stratos Gkagkanis, Michail E. Kiziroglou

Department of Automation Engineering T.E., ATEI Of Thessaloniki, 57400, Greece

***Abstract*—Applications using Photodiode Arrays demand accurate timing to control the duration of exposure and provide accurate frame time-stamping. In this paper, a real-time programming method used for a new medical laser scattering sensor system is described. In such devices, the margin of error must be small, so determinism is ensured and the code is optimized by exploitation of all available subsystems of the System on Chip, thereby speeding up various processes. A testing module has been fabricated to debug the driving system and ensure proper operation. Neither the algorithms nor the hardware configuration presented are bound to this particular device and can be used for any application using a sensor with the same operating principle.**

***Index Terms*—Analog-digital conversion, Microprocessors, Photodiodes**

I. Introduction

The work presented in this paper is part of a medical research device project for measuring laser scattering on blood cells [1], which involves a time critical process requiring fast and deterministic algorithms to drive a Photodiode Array (PDA).

The end goal is a routine, simple for the user to implement, without the need to change or even read the assembly instructions of the drivers running on the Programmable Realtime Units (PRUs).

II. Hardware In Use

The device is based on BeagleBone Black (BBB), a development platform which uses the AM3358 System on Chip (SoC) made by Texas Instruments (TI). The SoC is housing a significant number of subsystems with the most important for this application being the ARM Cortex-A8 running the OS and the routine coded in C, two 32-bit PRUs driving the PDA, an Interrupt Controller (INTC) for fast communication between the three CPUs, a 12-bit Analog to Digital Converter (ADC) for sampling the PDA output and the DDR RAM to temporary store the samples.

The PDA in use is the AMS TSL1401CL containing a linear array of 128 × 1 photodiodes evenly spaced on an area of 8 mm. [2]. The operating voltage in this application is 3.3 V but the ADC Analog Reference Voltage (V_{AREF}) is only 1.8 V. Signal conditioning is achieved with the help of a voltage divider connected to a circuit of voltage followers, linearly scaling down the Analog Output (AO) of the PDA to the voltage range of V_{AREF} while protecting the sensitive analog input of the chip.

Two signals are required for the PDA to work, a Serial-Input (SI) whose rising edge defines the start of a new cycle and a clock (CLK) to "clock out" samples one by one. In order to clock out a whole frame, one SI pulse is needed and 128 + 1 CLK pulses. The integration starts on the 19th CLK pulse and that during one integration cycle, the samples of the previous frame are being clocked out. In other words, the PDA handles two groups of data at the same time. It clocks out the previous frame while it integrates the current frame.

Even though all the subsystems mentioned above are important, the PRUs are those that handle all the time critical events. Two identical PRUs are included in the SoC with a 32-bit Load/Store architecture running at 200 MHz, with direct access to I/O and indirect access to most subsystems through external interconnects. Accessing those interconnects is the only way for the PRUs to reach the ADC and DDR, at the cost of losing determinism. For this reason, in the driver presented in this paper, the PRU0 does not access any interconnects and is only used to drive the PDA by generating SI and CLK signals. With every rising edge of CLK, PRU1 is informed through the INTC to collect and store samples from the PDA. In this way PRU0 maintains its deterministic characteristics while PRU1 handles asynchronous communication with necessary subsystems. The PRUs are equipped with volatile Instruction RAM instead of ROM, so the assembly code must be loaded to them every time by the ARM processor.

III. Capturing Frames

A vector of four arguments must be passed while calling the routine. The vector consists of the number of frames, integration time (T_{integr}) in microseconds (μs), frames per second (fps) and finally the CLK signal frequency in kHz. The duration of a frame cycle is the inverse of fps and is broken into three steps as illustrated in Fig. 1.: Integration, during which light is sampled, charging the PDA capacitors, Sampling, where integrated data are clocked out by PRU0 and sampled by PRU1, and a Delay step used for decoupling and independent control of the integration time and the frames per second parameters.

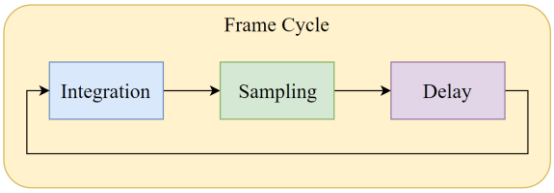

Fig. 1. Block diagram of a frame cycle showing its division into three steps.

It is important for every of the three steps to exist and be deterministic for the experimental data to be reliable. Integration duration is directly given as an argument, while Sampling and Delay duration is determined by the following equations [2]:

$$T_{Sampl} = \frac{1}{CLK \cdot 10^3} \cdot 129 + \frac{1}{CLK \cdot 250} \quad (1)$$

$$T_{Delay} = \frac{1}{fps} - T_{Sampl} - \left(T_{Integr} \cdot 10^{-6}\right) \quad (2)$$

With a 200 MHz clock, the instruction cycle period of the PRUs is 5 nanoseconds (ns) long. The time unit used by the ARM processor for the timing calculations, i.e. the implementation of delays between SI pulses during a sampling session, is the duration of 2 instructions, or 10 ns. This is because the PRU0 can count time in "delay loops" each of which comprises two instructions. All the calculations mentioned are done by the ARM processor on high level and are saved in the Shared RAM. Right after this is done, PRUs are loaded with their code, perform every initialization needed and get the values from the Shared RAM. Before starting the driving process, synchronization between the PRUs and the ARM processor is achieved with a handshake. When PRUs are done and all frames are saved in DDR RAM, PRU1 signals ARM to collect the data and store them in the SD card as a .txt file along with all the important information like fps, such that the data can be interpreted correctly with the appropriate tools.

IV. Testing & Debugging The System

For testing purposes, a prototype system has been fabricated which includes an Arduino board and three LEDs for testing as shown in Figure 3.

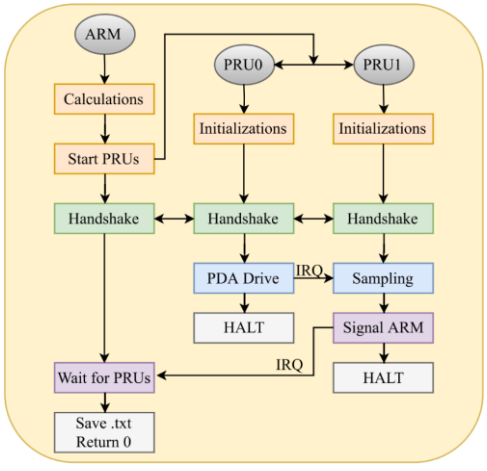

Fig. 2. Brief block diagram of the complete procedure.

The idea is to put the system inside a dark box with the LEDs right in front of the PDA and have the Arduino scan for SI pulses from the BBB. The aim of the test was to check whether the saved frames consist only of their own 128 pixels and no timing errors were made, such as mixing the first and last pixels of adjacent frames. The Arduino has been programmed to detect the rising edge of SI pulse and turn the LEDs on, in a way so every other frame would have all 128 pixels saturated and give the maximum value of 4095. In this way, the .txt file contains samples that alternate between the minimum and maximum value for every 128 of them. The results of the test made clear that conversion of the ADC had to be delayed for some microseconds due to the slew rate of the operational amplifiers.

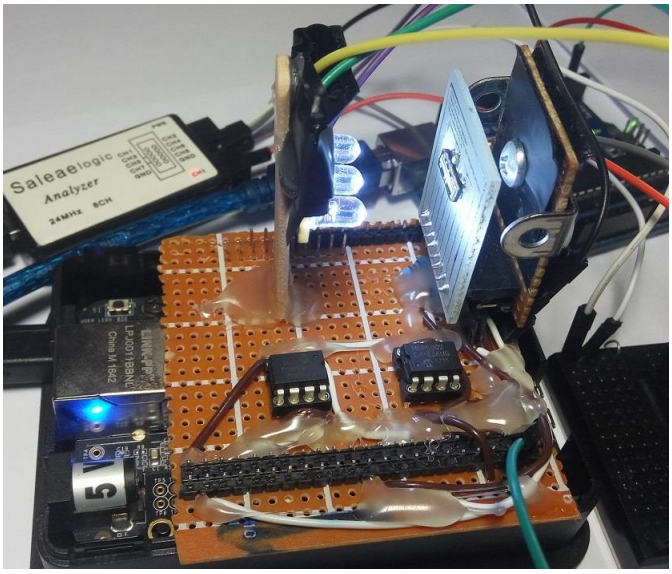

Fig. 3. Image of the prototype system with the LEDs on while debugging.

V. Conclusion and Outlook

In this work, fast, real-time sampling and storage has been achieved, by parallel programming two microcontrollers. This approach is practical, as systems with multiple cores, including microcontrollers are becoming widely available [3]. Advanced real-time control of sampling and controlling multiple signals may be possible by employing structured parallel programming techniques [3]. The developed technique will be used for implementing a laser-scattering based portable analyzer for biomedical applications.

References

[1] C. Iosifidis, K. Katsaliaki, P. Kollensperger and M. Kiziroglou, "Design of an embedded sensor system for measuring laser scattering on blood cells", In Proceedings of SPIE on Microtechnologies, 2017.
[2] AMS, "TSL1401CL 128 x 1 Linear Sensor Array with Hold" TSL1401 datasheet, Aug. 2016.
[3] Beaglebone Black Platform, Dec. 2017, https://beagleboard.org/black.
[4] P. LeGuernic, T. Gautier, M. Le Borgne and C. Le Maire, Programming real-time applications with SIGNAL, Proceedings of the IEEE, 79 (9), 1321 – 1336, 1991.